

Influence of Mg-to-Ce Concentration Ratio on Cathodoluminescence in LuAG and LuGAGG Single-Crystalline Films

Ondrej Lalinsky,* Petr Schauer, and Miroslav Kucera

The cathodoluminescence (CL) characterizations of $\text{Lu}_3\text{Al}_5\text{O}_{12}:\text{Ce},\text{Mg}$ (LuAG:Ce,Mg) and of multicomponent $(\text{Lu}_{0.25}\text{Gd}_{0.74})_3(\text{Ga}_{2.48}\text{Al}_{2.52})\text{O}_{12}:\text{Ce},\text{Mg}$ (LuGAGG:Ce,Mg) single-crystalline garnet films are supported by the optical absorption spectroscopy. Using this approach, the influence of the Mg-to-Ce concentration ratio on the CL spectra and the CL decay is analyzed. The crucial role of stable Ce^{4+} centers in CL is shown in Mg-rich film studies. Although the CL intensity is somewhat reduced, drastic improvements in timing performance are demonstrated, including the CL decay time as low as 4.2 ns and the afterglow as low as 0.015% at 500 ns after the e-beam excitation cutoff. These results predetermine the utilization of the LuAG:Ce,Mg and LuGAGG:Ce,Mg single-crystalline films in e-beam detection systems, where especially fast scintillator response is crucial.

1. Introduction

In applications of scintillators for electron detection, such as electron microscopy and e-beam inspection, the essential scintillator parameters are the very fast scintillation decay and high dynamic range.^[1,2] Also, a high light yield (LY) is required, but more important is the high signal-to-noise ratio.^[3] Recently, with the use of balanced admixture engineering in cerium-doped multicomponent garnet scintillators, the cathodoluminescence (CL) decay time as low as 28 ns and the CL afterglow as low as 0.01% (at 1 μs after excitation) were reported under e-beam excitation.^[4] Very favorable properties were also found in photoluminescence (PL) studies of other garnet specimens, where the improvement of the LY (doubled to more than 50 000 photon MeV^{-1}) and substantial suppression of the unwanted afterglow were achieved in Gd- and

Ga-substituted multicomponent garnets $(\text{LuGd})_3(\text{GaAl})_5\text{O}_{12}:\text{Ce}$ (LuGAGG:Ce).^[4–6] In spite of all the aforementioned progress, the decay time in particular is still too long for some e-beam detection systems.

This problem can be solved by co-doping the garnet with Mg^{2+} . This leads to additional afterglow reduction in LuGAGG:Ce,^[7–9] and especially in $\text{Lu}_3\text{Al}_5\text{O}_{12}:\text{Ce}$ (LuAG:Ce) systems,^[10–12] to both rise and decay time reduction,^[13] but also, unluckily, to LY reduction at higher Mg co-doping. The afterglow suppression was explained by the Ce^{4+} center stabilization, competing better with electronic traps for charge capture, which resulted in practical inactivation of shallow traps. The Ce^{4+} center

has practically the same emission characteristic as Ce^{3+} .^[10,14] However, the LY decrease, along with the decreasing intensity of the stable Ce^{3+} content, may prompt questions such as: Will the Ce^{3+} emission be sustained even if all the Ce ions are stabilized at the charge state of 4+, and do the stable Ce^{4+} centers even participate in the Ce^{3+} 5d–4f emission? These questions were positively answered in some Mg-rich single crystals,^[11] but not yet in the single-crystalline films or ceramics.

Moreover, the CL has not been studied in LuAG:Ce,Mg films; only studies of the PL, radioluminescence (RL), scintillation properties (LY, scintillation decay), and related studies were conducted.^[12] The PL is extremely weak in the Mg-rich films because the Ce^{3+} absorption bands disappear almost completely. The RL study could be satisfactory at this stage, but X-rays have high penetration depth so that a substrate can also be excited. The CL study solves both of these problems. First, the e-beam of 10 keV has enough energy to excite electrons across the garnet bandgap. Second, the penetration depth of the 10 keV electrons is around 1 μm in garnets,^[15] which is sufficient for the study of films with thicknesses of around 10 μm .

The aim of this work is to study the influence of the Mg-to-Ce concentration ratio on CL characteristics in LuAG:Ce,Mg and in multicomponent LuGAGG:Ce,Mg in an effort to shorten the CL decay and to confirm the crucial role of the stable Ce^{4+} centers in the Ce^{3+} emission. For these reasons, two series of LuAG:Ce,Mg and multicomponent LuGAGG:Ce,Mg single-crystalline thin films were prepared with various concentrations of Mg^{2+} ions, including Mg-rich films.

O. Lalinsky, Dr. P. Schauer
Institute of Scientific Instruments
Czech Academy of Sciences
Kralovopolska 147, Brno 612 64, Czech Republic
E-mail: xodr@isibrno.cz

Prof. M. Kucera
Faculty of Mathematics and Physics
Charles University
Ke Karlovu 5, Praha 2 121 16, Czech Republic

 The ORCID identification number(s) for the author(s) of this article can be found under <https://doi.org/10.1002/pssa.201801016>.

DOI: 10.1002/pssa.201801016

2. Results and Discussion

The optical absorption spectra of the LuAG:Ce,Mg and LuGAGG:Ce,Mg epitaxial films are shown in **Figure 1**. The broad spectral bands in absorption at 440 and 345 nm correspond to the allowed $4f-5d_1$ and $4f-5d_2$ (Ce^{3+}) transitions, respectively. The intensities of both these structures gradually decrease with increasing Mg^{2+} concentration. In contrast, the intensity of the broad absorption band in the UV spectrum region (below ≈ 300 nm) increases with an increase in the Mg^{2+} concentration. Such intense UV absorption originates from the charge transfer (CT) of an electron from oxygen ligands toward tetravalent Ce^{4+} ions, which arises due to the necessity of the charge compensation of the aliovalent Mg^{2+} ions embedded in trivalent sites.^[8] It is worth mentioning that the LuAG:Ce,Mg film with the highest Mg content of 0.11 at% is completely transparent in the visible range without any noticeable absorption at 445 nm, which confirms that virtually all cerium ions were stabilized in the $4+$ charge state. In this film, the analyzed Mg-to-Ce stoichiometric ratio is indeed slightly higher than 1. Although the specimens were grown in the oxidizing atmosphere, the creation

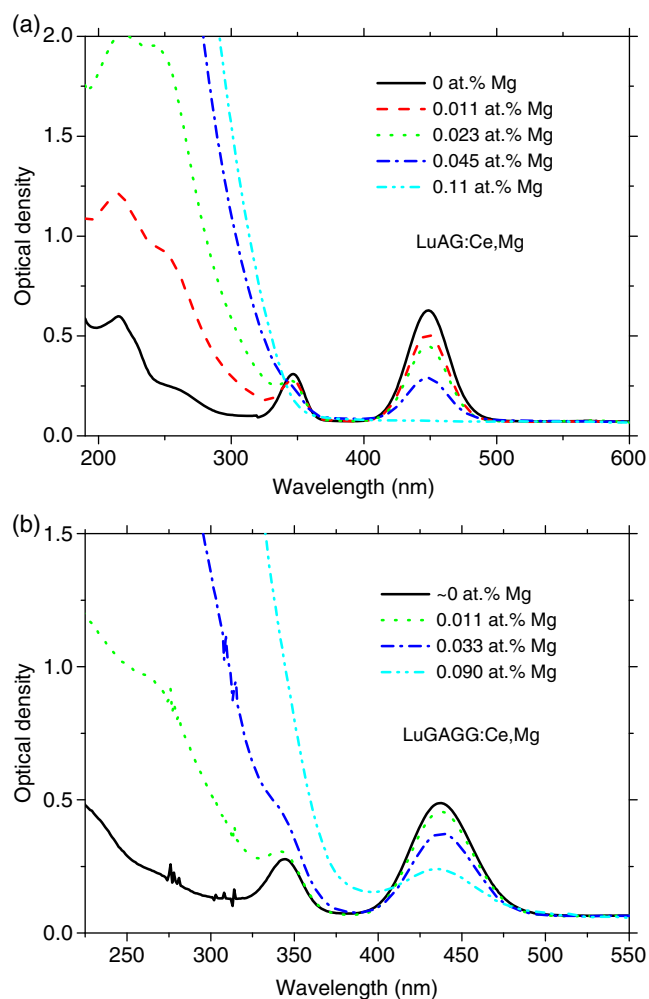


Figure 1. The optical absorption spectra of a) LuAG:Ce,Mg and b) LuGAGG:Ce,Mg single-crystalline films.

of oxygen vacancies cannot be excluded at higher Mg concentrations. Any F^{+} - or F-related defect emission was not observed in the studied specimens; in contrast, there can be some stable Ce^{4+} ions even in the Mg-free specimens.^[16] The weak sharp lines observed around 275 and 310 nm in the LuGAGG:Ce, Mg spectra correspond to spin and parity forbidden $4f-4f$ transition, $^8S \rightarrow ^6I_1$, and $^8S \rightarrow ^6P_1$, respectively, in the Gd^{3+} ions.^[17]

The CL spectra of the studied specimens are shown in **Figure 2**. The spectra are dominated by a doublet with a maximum around ≈ 520 nm, which corresponds to the $5d_1-4f$ (Ce^{3+}) transitions. In the LuAG:Ce,Mg films, the integral intensity of the characteristic Ce^{3+} emission is still comparable with the integral intensity of the reference $Bi_4Ge_3O_{12}$ (BGO) specimen even for the highest Mg concentration (0.11 at% Mg, 1LM9) where no trivalent Ce^{3+} ions are present, as shown in **Table 1** and Figure 2a. This is in agreement with the previous RL studies of LuAG:Ce,Mg single crystals.^[11] The weak broad UV emission band centered around ≈ 300 nm in Mg-free

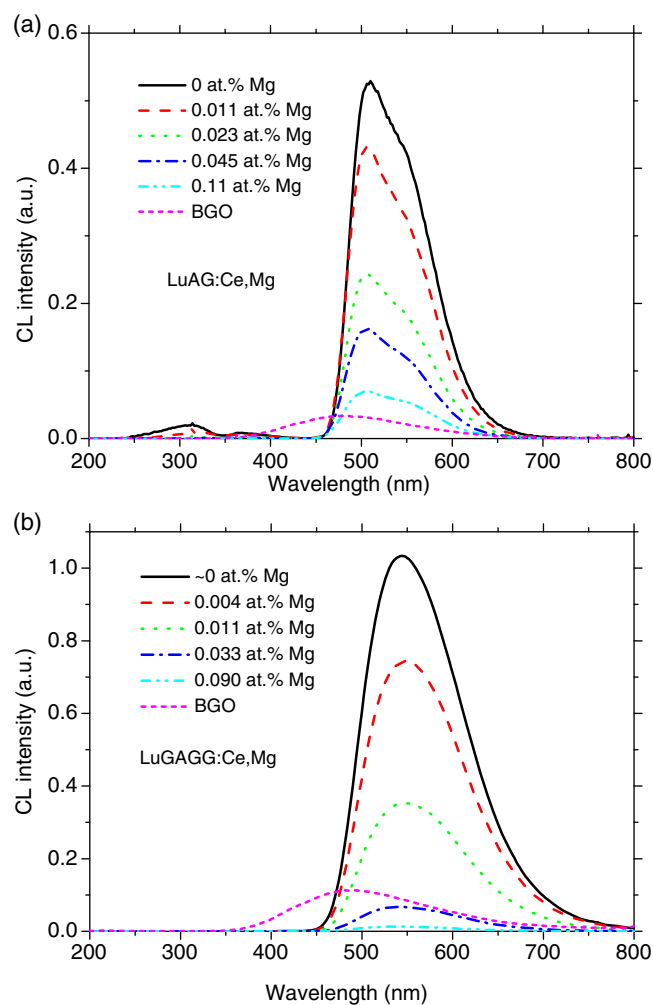


Figure 2. The CL emission spectra of a) LuAG:Ce,Mg and b) LuGAGG:Ce, Mg single-crystalline films with various Mg concentrations. The spectra were corrected for the apparatus spectral transmittance and for the photodetector spectral sensitivity. The reference BGO spectrum is also shown for comparison.

Table 1. Parameters of the LuAG:Ce,Mg (1LM) and LuGAGG:Ce,Mg (1LGM) multicomponent single-crystalline films.

Specimen sign	Thickness ^{a)} [μm]	Mg concentration ^{b)} [at%]	Relative CL intensity ^{c)}	τ_1/A_1 ^{d)} [ns]	τ_2/A_2 ^{d)} [ns]	τ_3/A_3 ^{d)} [ns]	τ_4/A_4 ^{d)} [μs]	AG ^{e)} [%]
1LM1	30.0	0	9.6	14/0.42	63/0.50	–	–	4.7
1LM4	22.0	0.011	7.6	13/0.37	56/0.57	540/0.047	2.0/0.011	2.7
1LM5	22.0	0.023	4.2	7.7/0.19	40/0.73	160/0.065	0.71/0.014	0.97
1LM7	17.0	0.045	2.8	8.2/0.43	41/0.56	260/0.011	–	0.17
1LM9	9.4	0.11	1.3	7.5/0.46	34/0.53	110/0.010	–	0.015
1LGM3	16.3	≈0 ⁰⁾	6.3	21/0.34	74/0.62	280/0.039	–	0.72
1LGM7	16.8	0.004	4.7	22/0.43	63/0.54	230/0.029	–	0.35
1LGM8	16.7	0.011	2.2	12/0.60	53/0.39	210/0.011	–	0.11
1LGM10	16.7	0.033	0.41	6.6/0.63	32/0.37	–	–	0.054
1LGM11	11.9	0.090	0.08	4.2/0.93	20/0.072	–	–	0.13

^{a)}Film thickness; ^{b)}Element concentration in the Lu₃Al₅O₁₂:Ce,Mg (1LM) and (Lu_{0.25}Gd_{0.74})₃(Ga_{2.48}Al_{2.52})O₁₂:Ce,Mg (1LGM) films. 1LM films contain 0.11 at% Ce, 1LGM films contain 0.15 at%; ^{c)}CL intensity integrated over the 200–800 nm range and related to the integral CL intensity of BGO; ^{d)}Fit decay constants obtained from the fitted decay curves by Equation (1); ^{e)}Afterglow at 500 ns after e-beam excitation cutoff represented by the $I(t)$ in Equation (1); ⁰⁾The specimen may contain accidental impurity up to several millionth at% Mg that is below the resolution of concentration detection methods and CL experiments—the specimen can be considered to be Mg-free.

LuAG:Ce, as shown in Figure 2a, comes from the host-defect emission.^[14] This emission was largely suppressed by Mg co-doping.

The situation looks different in the multicomponent LuGAGG:Ce,Mg films. The Ce³⁺ 4f–5d absorption is present even in the Mg-rich 1LGM11 (0.090 at% Mg) specimen, as shown in Figure 1b. Therefore, some Ce³⁺ ions are still present. It can be expected because the Mg/Ce concentration ratio is 0.6. However, the Ce³⁺ 5d–4f emission almost vanished in this specimen, as shown in Table 1 and Figure 2b. The noticeably decreased CL intensity of the multicomponent LuGAGG:Ce, Mg films in comparison with the LuAG:Ce,Mg films can be explained as an association of two phenomena. First, the Gd³⁺ sublattice, in combination with Ce⁴⁺ centers, may create some nonradiative pathways that decrease the luminescence output.^[8] This phenomenon depends on the Mg²⁺ concentration. Second, it can be the effect of the Al/Ga and Lu/Gd substitution used in the so-called “band-gap engineering strategy.”^[18] The Ga³⁺ substitution shifts down the bottom of the conduction band, buries shallow electron trap levels in it, and thus diminishes their influence on the CL. The Gd³⁺ substitution should prevent from doing the same to the Ce³⁺ 5d levels by shifting them down. Therefore, the CL intensity of the Ce³⁺ emission can be lower in Ga-substituted specimens due to higher probability of ionization of the Ce³⁺ excited state. This effect was observed in GAGG:Ce films in our previous study.^[19] The ionization of the Ce³⁺ excited state should not depend on the Mg²⁺ concentration, but can still contribute to the CL intensity decrease of all studied LuGAGG:Ce,Mg films, compared to the relative CL intensity of the 1LM1 with the 1LGM3 (Mg-free specimens) in Table 1.

Experimental data and CL decay curves obtained by the deconvolution of the data using the sum of power-law and multiexponential functions

$$I(t) = I_0 + A_0(t + t_0)^{-p} + \sum_i A_i \exp(-t/\tau_i) \quad (1)$$

are displayed in Figure 3. The I_0 parameter represents the level of background electronic noise, and A_i is the relative intensity of the i -th exponential component with the decay constant τ_i . These parameters are summarized in Table 1. The parameters A_0 , t_0 , and p are related to an extra power-law function. This function was used only in the case of the 1LM1 film (Mg-free LuAG:Ce). The power-law function describes the sub-gap tunneling-driven radiative recombination between a cerium center and a nearby lying shallow electron trap in the LuAG:Ce single crystal.^[20] However, it possesses the physical meaning only when the value of the p parameter is within the interval of 0.95–1.5.^[21] Among the studied specimens, only the 1LM1 film (Mg-free LuAG:Ce) fulfilled this criterion as it shows a p parameter value of 1.49. All other films showed it to be around 2.5 (fits not shown), so only the multiexponential fit was used in such a case. This may indicate that substantial tunneling from an electron trap occurs only in the 1LM1 film (Mg-free LuAG:Ce) and, with the increasing Mg content, this tunneling continuously diminishes.

The gradual suppression of the afterglow (defined here as the CL intensity at 500 ns after e-beam excitation cutoff) with the increasing Mg-to-Ce concentration ratio is observed in Figure 3a in the LuAG:Ce,Mg films. Five hundred nanoseconds was selected as a practical value for scanning (transmission) electron microscope (S(T)EM) and some other e-beam devices. The gradual decrease of decay times of all components and relative intensity decrease of slower decay components are shown in Table 1. The slow components are caused by delayed recombination at the Ce³⁺ centers of charge captured and thereafter released from the electron traps. The effect of Mg co-doping in the films was explained by the Ce³⁺ → Ce⁴⁺ centers stabilization, which should better compete with the shallow electron traps for electron capture.^[8] This diminishes also the effect of tunneling. It is not because an electron has lower probability of tunneling from a trap, but because of lower trapping probability. Then, the influence of the traps on the CL decreases with increasing Mg content and, consequently, the intensities of the slow decay components also decrease.

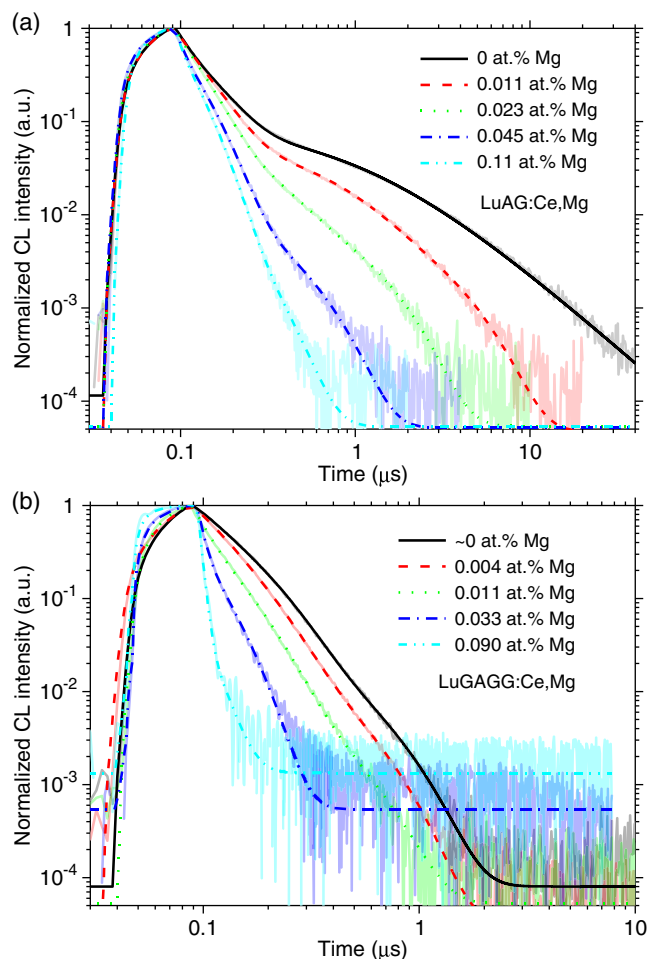


Figure 3. The spectrally unresolved CL decays of a) LuAG:Ce,Mg and b) LuGAGG:Ce,Mg single-crystalline films under pulsed e-beam excitation. The semitransparent solid lines are measured data. The deep lines of different styles are the result of a fit and represent the convolution of Equation (1) in the text with the instrumental response function.

In the multicomponent LuGAGG:Ce,Mg films, noticeable afterglow suppression is observable in the specimens with Mg content up to 0.011 at%, as shown in Figure 3b and Table 1. This is probably due to the $Ce^{3+} \rightarrow Ce^{4+}$ centers stabilization. Similar afterglow suppression in the LuGAGG:Ce,Mg single-crystalline films has been published previously.^[8] Moreover, the afterglow is already well suppressed in the Mg-free 1LGM3 specimen in comparison with LuAG:Ce,Mg films. This may be due to the aforementioned Ga^{3+} ions reducing the effect of the electron traps. We note that the increase in the background signal (and afterglow value in Table 1) in the Mg-rich specimens (≥ 0.033 at% Mg) is due to the very weak CL signal of these specimens.

The general acceleration of the CL decay components with the increasing Mg content is observable both in the LuAG:Ce,Mg and LuGAGG:Ce,Mg films in Figure 3 and Table 1, where the τ_i fit decay constants from Equation (1) gradually decrease with the increase in the Mg content. This may be caused by a nonradiative recombination pathway at the centers

that are formed due to the presence of Mg^{2+} .^[10] The nature of the centers formed at the excess of Mg^{2+} ions in the films was frequently discussed in the literature. Among the hypotheses is the formation of O^- -like centers (a migrating hole trapped by the oxygen sublattice). These centers were proven by the electron paramagnetic resonance in LuAG:Ce,Mg single-crystals and ceramics,^[22–25] and they can act as nonradiative centers causing a light loss.^[23,25] Furthermore, at higher Mg concentrations, oxygen vacancies, constituting deep electron traps, can also be formed. The nonradiative recombination prevails in the films with higher Mg content, and it is in good agreement with the decreasing CL intensity in Figure 2 and with the increasing level of electronic noise represented by the I_0 parameter in Equation (1), as shown in Figure 3b.

In comparison with the CL decay of the 1LM1 film (Mg-free LuAG:Ce), the decay of the 1LGM3 film (≈ 0 at% Mg) is composed of relatively slower first and second exponential decay components, as shown in Table 1. These two exponentials are the main components of the $Ce^{3+} 5d-4f$ emission, and the slowdown of these components was interpreted in similar systems as being due to energy migration over the Gd^{3+} sublattice, followed by energy transfer to Ce^{3+} .^[26] As the CL decay of the studied films accelerates with the increasing Mg content, the slow components gradually disappear, and fewer exponentials to the proper data fit are required. Such a difference in the function approximation may cause a small variation in the obtained decay times. This is definitely the case of the 1LM7 film (0.045 at% Mg), where its decay is faster than decay of the 1LM5 film. Decay constants τ_i of the 1LM5 are shorter than that of the 1LM7. However, these two facts are not contradictory because relative amplitude A_1 of the fastest component is significantly higher for the 1LM7 than for the 1LM5. For the 1LGM10 (0.033 at% Mg) and 1LGM11 (0.090 at% Mg) specimens, fewer necessary exponentials can also be caused by the increased electronic noise level represented by the I_0 parameter in Equation (1) in comparison with the other curves in Figure 3. Such noise buries potentially slower components and is caused by the very low CL intensity of these films (Figure 2b), as mentioned earlier.

In previous articles, a reduction in the rise time to tens of picoseconds with the increasing Mg content was demonstrated.^[13,27] However, this could not be observed using our setup because the minimum width of the excitation e-beam pulse was 50 ns. The rise of the scintillation signal and its faster saturation observed especially in LuGAGG:Ce,Mg system, Figure 3b, correlates well with the faster decay time in heavily Mg-doped specimens.

3. Conclusion

In this article, we studied the CL properties in LuAG:Ce,Mg and multicomponent LuGAGG:Ce,Mg garnet single-crystalline films supported by the optical absorption spectra. The crucial role of the Ce^{4+} ions was shown in heavily Mg^{2+} co-doped specimens, where the $Ce^{3+} 5d-4f$ emission is still present under e-beam excitation, although almost all Ce ions were stabilized in the 4+ charge state. This was demonstrated in the 1LM9 specimen (0.11 at% Mg), where the Mg-to-Ce concentration ratio was ≈ 1 .

In the LuGAGG:Ce,Mg films, not all the Ce ions were stabilized in the 4+ charge state because the highest Mg-to-Ce concentration ratio in the films was ≈ 0.6 (1LGM11). Nevertheless, the $Ce^{3+} 5d-4f$ emission almost vanished in this specimen. The acceleration of the CL decay, the suppression of the afterglow, and the decrease of the CL intensity were presented as the main effects of the Mg co-doping, both in the LuAG:Ce, Mg and LuGAGG:Ce,Mg films. These effects correlate well with previous luminescence findings under X-ray and/or α -particle excitations.^[8,12] The loss of the LY is an undesirable effect for possible application, and so we admit the lower potential to apply the LuAG:Ce,Mg and the LuGAGG:Ce,Mg single-crystalline films in many areas. However, these materials can be perspective fast scintillators for applications where the fastest possible response and low afterglow are crucial, and a somewhat reduced intensity can be acceptable. Optimum Mg-doping level depends on application and it somewhat differs for LuAG:Ce,Mg and LuGAGG:Ce,Mg. The films with ≈ 0.015 at% Mg could be perspective scintillators for detectors in real-time diagnostics in e-beam inspection systems. Higher doping level (0.030–0.045 at% Mg) could be appreciated in the detectors of high-energy particles/photons.

4. Experimental Section

Mg-co-doped LuAG:Ce0.7% and LuGAGG:Ce1% (relative concentrations in the dodecahedral sites) single-crystalline epitaxial films were grown by the isothermal dipping liquid-phase epitaxy on undoped LuAG and GAGG substrates, respectively, of (111) and (100) crystallographic orientations. The compositions of specimens, which were determined by the electron-probe microanalysis and glow-discharge mass spectrometry, and the decay times obtained from the fit are shown in Table 1. Special attention was paid to the purity of the films and the elimination of any potential impurities from the flux. The films were grown from lead-free BaO–B₂O₃–BaF₂ flux. Starting raw materials of 5N purity were used. Technical details were published in previous studies.^[28,29] The thicknesses of the films were 9.4–30 μ m. The growth temperatures were (1030 ± 1) °C. The films had a single-crystalline and single-phase form, as proven by X-ray diffraction. The set of specimens included a reference single crystal of BGO that had an LY of 8000 photons MeV⁻¹. All the specimens were coated with 50 nm of Al to prevent surface charging. Optical absorption spectra, CL spectra, and CL decays were measured. The experimental setups were described in previous studies.^[30,31] The CL spectra were measured under the continuous excitation of an electron beam with an energy of 10 keV and a current of 30 nA. The e-beam spot was 2 mm in diameter. For the CL decays, the electron beam was periodically deflected out of the specimen by an electrostatic deflection system, which enabled the creation of e-beam pulses with the repetition rate of 1 kHz, pulse width of 50 ns, and current of 150 nA. All the experiments were performed at room temperature.

Acknowledgements

The research was supported by the Czech Science Foundation (project, GA16-05631S and GA16-15569S—growth of specimens) and by the Ministry of Education, Youth and Sports of the Czech Republic (project LO1212). The research infrastructure was funded by the Ministry of Education, Youth and Sports of the Czech Republic, and the European Commission (project CZ.1.05/2.1.00/01.0017). The authors thank the Institute of Physics at the Czech Academy of Sciences for lending the BGO specimen.

Conflict of Interest

The authors declare no conflict of interest.

Keywords

cathodoluminescence, co-doping, multicomponent garnet, scintillator, single-crystalline film

Received: December 20, 2018

Revised: May 20, 2019

Published online: July 15, 2019

- [1] J. I. Goldstein, D. E. Newbury, J. R. Michael, N. W. Ritchie, J. H. J. Scott, D. C. Joy, *Scanning Electron Microscopy and X-Ray Microanalysis*, Springer, Berlin, New York **2017**.
- [2] T. Hirano, S. Yamaguchi, M. Naka, M. Itoh, M. Kadowaki, T. Koike, Y. Yamazaki, K. Terao, M. Hatakeyama, H. Sobukawa, *Proc SPIE* **2010**, 7823, 2C.
- [3] D. C. Joy, C. S. Joy, R. D. Bunn, *Scanning* **1996**, 18, 533.
- [4] P. Schauer, O. Lalinsky, M. Kucera, Z. Lucenicova, M. Hanus, *Opt. Mater.* **2017**, 72, 359.
- [5] P. Prusa, M. Kucera, J. A. Mares, Z. Onderisinova, M. Hanus, V. Babin, A. Beitlerova, M. Nikl, *Cryst. Growth Des.* **2015**, 15, 3715.
- [6] Y. Zorenko, V. Gorbenko, T. Zorenko, O. Sidletskiy, A. Fedorov, P. Bilski, A. Twardak, *Phys. Status Solidi-Rapid Res. Lett.* **2015**, 9, 489.
- [7] K. Kamada, Y. Shoji, V. V. Kochurikhin, A. Nagura, S. Okumura, S. Yamamoto, J. Y. Yeom, S. Kurosawa, J. Pejchal, Y. Yokota, Y. Ohashi, M. Nikl, M. Yoshino, A. Yoshikawa, *IEEE Trans. Nucl. Sci.* **2016**, 63, 443.
- [8] P. Prusa, M. Kucera, V. Babin, P. Bruza, D. Panek, A. Beitlerova, J. A. Mares, M. Hanus, Z. Lucenicova, M. Nikl, T. Parkman, *Adv. Opt. Mater.* **2017**, 5, 9.
- [9] K. Kamada, Y. Shoji, V. V. Kochurikhin, A. Nagura, S. Okumura, S. Yamamoto, J. Y. Yeom, S. Kurosawa, J. Pejchal, Y. Yokota, Y. Ohashi, M. Nikl, M. Yoshino, A. Yoshikawa, *J. Cryst. Growth* **2017**, 468, 407.
- [10] S. P. Liu, X. Q. Feng, Z. W. Zhou, M. Nikl, Y. Shi, Y. B. Pan, *Phys. Status Solidi-Rapid Res. Lett.* **2014**, 8, 105.
- [11] M. Nikl, K. Kamada, V. Babin, J. Pejchal, K. Pilarova, E. Mihokova, A. Beitlerova, K. Bartosiewicz, S. Kurosawa, A. Yoshikawa, *Cryst. Growth Des.* **2014**, 14, 4827.
- [12] P. Prusa, M. Kucera, V. Babin, P. Bruza, T. Parkman, D. Panek, A. Beitlerova, J. A. Mares, M. Hanus, Z. Lucenicova, M. Pokorny, M. Nikl, *Cryst. Growth Des.* **2018**, 18, 4998.
- [13] M. T. Lucchini, V. Babin, P. Bohacek, S. Gundacker, K. Kamada, M. Nikl, A. Petrosyan, A. Yoshikawa, E. Auffray, *Nucl. Instrum. Methods Phys. Res. Sect. A-Accel. Spectrom. Dect. Assoc. Equip.* **2016**, 816, 176.
- [14] S. R. Rotman, H. L. Tuller, C. Warde, *J. Appl. Phys.* **1992**, 71, 1209.
- [15] P. Schauer, J. Bok, *Nucl. Instrum. Methods Phys. Res. Sect. B-Beam Interact. Mater. Atoms* **2013**, 308, 68.
- [16] Y. T. Wu, J. L. Luo, M. Nikl, G. H. Ren, *APL Mater.* **2014**, 2, 8.
- [17] M. Kucera, M. Nikl, M. Hanus, Z. Onderisinova, *Phys. Status Solidi-Rapid Res. Lett.* **2013**, 7, 571.
- [18] M. Fasoli, A. Vedda, M. Nikl, C. Jiang, B. P. Uberuaga, D. A. Andersson, K. J. McClellan, C. R. Stanek, *Phys. Rev. B* **2011**, 84, 4.
- [19] J. Bok, O. Lalinsky, M. Hanus, Z. Onderisinova, J. Kelar, M. Kucera, *Ultramicroscopy* **2016**, 163, 1.

- [20] M. Nikl, A. Vedda, M. Fasoli, I. Fontana, V. V. Laguta, E. Mihokova, J. Pejchal, J. Rosa, K. Nejezchleb, *Phys. Rev. B* **2007**, 76, 8.
- [21] D. J. Huntley, *J. Phys.-Condes. Matter* **2006**, 18, 1359.
- [22] M. Nikl, V. Babin, J. Pejchal, V. V. Laguta, M. Buryi, J. A. Mares, K. Kamada, S. Kurosawa, A. Yoshikawa, D. Panek, T. Parkman, P. Bruza, K. Mann, M. Muller, *IEEE Trans. Nucl. Sci.* **2016**, 63, 433.
- [23] C. Hu, S. P. Liu, M. Fasoli, A. Vedda, M. Nikl, X. Q. Feng, Y. B. Pan, *Phys. Status Solidi-Rapid Res. Lett.* **2015**, 9, 245.
- [24] C. Hu, S. P. Liu, M. Fasoli, A. Vedda, M. Nikl, X. Q. Feng, Y. B. Pan, *Opt. Mater.* **2015**, 45, 252.
- [25] V. Laguta, M. Buryi, J. Pejchal, V. Babin, M. Nikl, *Phys. Rev. Appl.* **2018**, 10, 034058.
- [26] M. Nikl, A. Yoshikawa, *Adv. Opt. Mater.* **2015**, 3, 463.
- [27] G. Tamulaitis, A. Vaitkevicius, S. Nargelas, R. Augulis, V. Gulbinas, P. Bohacek, M. Nikl, A. Borisevich, A. Fedorov, M. Korjik, E. Auffray, *Nucl. Instrum. Methods Phys. Res. Sect. A-Accel. Spectrom. Dect. Assoc. Equip.* **2017**, 870, 25.
- [28] M. Kucera, K. Nitsch, M. Kubova, N. Solovieva, M. Nikl, J. A. Mares, *IEEE Trans. Nucl. Sci.* **2008**, 55, 1201.
- [29] M. Kucera, K. Nitsch, M. Nikl, M. Hanus, S. Danis, *J. Cryst. Growth* **2010**, 312, 1538.
- [30] J. Bok, P. Schauer, *Meas. Sci. Technol.* **2014**, 25, 7.
- [31] M. Kucera, M. Nikl, M. Hanus, Z. Onderisnova, A. Beitlerova, *IEEE Trans. Nucl. Sci.* **2012**, 59, 2275.